

Ultrafast surface plasmon-polariton interference and switching in multiple crossing dielectric waveguides

Tobias Birr¹ · Urs Zywiets¹ · Tim Fischer¹ · Parva Chhantyal¹ · Andrey B. Evlyukhin¹ · Boris N. Chichkov¹ · Carsten Reinhardt¹

Received: 19 August 2015 / Accepted: 9 May 2016 / Published online: 27 May 2016
© Springer-Verlag Berlin Heidelberg 2016

Abstract In this paper, we investigate propagation effects and interference switching of surface plasmon-polaritons (SPPs) in a junction of multiple crossed waveguides. These waveguides are produced on a thin gold layer by a simple photolithographic procedure. The waveguide dimensions are optimized for SPP excitation and propagation along two crossed input waveguides. At the waveguide intersection, different possibilities for SPP propagation into multiple output waveguides are offered. Using leakage radiation microscopy, we find that the SPPs preferably propagate into only one specific direction different from the direction of the input waveguides with avoidance of signal backscattering into the input direction. Furthermore, it is demonstrated that the SPP intensity at the output waveguide can be tuned by interference effects induced by a phase shift of the excitation laser beams. Additionally, we study the influence of different angles between the two input and the one specific output waveguides of the junction structure on the propagation properties of SPP modes in order to demonstrate a highest possible energy flux into the output waveguide. The experimental investigations are supported by finite-difference time-domain simulations. Good agreement between experimental results and numerical simulations is obtained. Applications of this effect are discussed for realization of ultrafast optical/plasmonic switches and optical logic gate structures with potential for integration and cascading.

1 Introduction

The twenty-first century is named as the century of photonics, including optical communication systems, photonic integrated circuits, and optical computing, allowing for ultrafast and broadband purely optical data transport and processing [1]. This requires the development of all-optical switching elements and logic gate structures. Using photons as information carriers, instead of electrons, would not only drastically increase the available information bandwidth, but it would also help to overcome interconnect delays and heat generation associated with conventional integrated electronic circuits [2].

To achieve optical switching, two main routes have been followed in scientific literature: the use of nonlinear processes and application of linear optical interference effects [3–11]. Especially optical interference, due to low required light intensities [7, 12, 13], appears very promising and will be considered in this paper.

With respect to comparable integration capacities, the substitution of electronic switching and computing units by photonic integrated circuits remains a challenging task, due to the existing size mismatch of electronic components and photonic modes. The diffraction limit sets severe restrictions on further reducing dimensions of optical circuitry down to electronic length scales. Up to now, there are only few experimental demonstrations of low-loss, nanoscale, all-optical switching elements and logic devices which are suitable for on-chip integration [9, 14].

A promising approach for achieving high integration of photonic components is based on surface plasmon-polaritons (SPPs) [2, 15–17]. Different types of SPP waveguide concepts, enabling confined SPP guiding for data transport applications, such as channel plasmon-polaritons [18, 19], metal-insulator-metal structures [20], metal strips and

This article is part of the topical collection “Ultrafast Nanooptics” guest edited by Martin Aeschlimann and Walter Pfeiffer.

✉ Tobias Birr
t.birr@lzh.de

¹ Laser Zentrum Hannover e.V., Hollerithallee 8,
30419 Hannover, Germany

nanowires [21], and dielectrically loaded SPP waveguides (DLSPWs) [22–24], have been proposed and investigated. Alternative schemes include long-range surface plasmon-polaritons (LRSPPs) [25–27], nanoparticle chains [28–31], and periodically structured metal surfaces, exhibiting band-gaps for SPPs [32–35].

Interference switching and realization of logic operations employing surface plasmons has previously been investigated using nanowires, plane metal surfaces, and slot waveguides [1, 2, 36, 37]. However, these approaches have certain disadvantages concerning the fabrication process, e.g., nanowire structures have been formed by chance, and precise slot waveguide fabrication requires expensive and time-consuming ion beam lithography.

To further fulfill the requirements for logic gate operations, the proposed SPP switches should exhibit several basic properties as they are given in Ref. [38]. The most important conditions are cascability, fan-out, i.e., one logic or switching stage should provide enough output signal/energy to drive at least two new inputs, and isolation of input ports from output ports, i.e., avoidance of back-reflections of plasmonic signals into the input ports. Inherent to plasmonic interference switching for the realization of optical logic operations is a critical biasing, meaning that the operation point, i.e., the relative phase of two interfering SPPs has to be set with a certain precision. Nevertheless, SPP switching elements, whose logic operation remains independent of ohmic losses, can be constructed.

In this paper, we present experimental investigations and numerical simulations on coherent SPP propagation and interference interaction in a junction of multiple crossed dielectrically loaded waveguides, acting as switching and logic optical elements. Interference of coherent fundamental SPP waveguide modes in complex dielectric guiding structures will be applied to avoid signal backscattering and to enhance output SPP signal levels, providing the possibility for cascading logic operational elements.

The multiple waveguide junction resembles a star-like dielectrically loaded plasmonic waveguide structure, shown in Fig. 1a, where different propagation directions for the in-coupled SPP waveguide modes are offered at the junction region.

The basic structure consists of two diagonal dielectrically loaded SPP waveguides, intersecting each other under an angle of 90° as indicated in Fig. 1b. These two diagonal waveguides are also referred to as the input waveguides. From the intersection point, four additional waveguides extend straight to the top, right, bottom, and left. Fabrication of such complex waveguide structures presented in this contribution is performed using microscope projection photolithography (MPP) with resolutions down to 230 nm, which is described in the experimental details (Sect. 2).

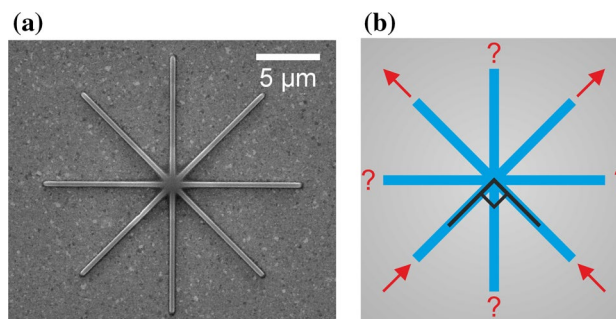


Fig. 1 **a** Scanning electron microscope image of the multiple waveguide junction structure made from Ormosil on a thin gold layer atop a standard microscopic cover glass. Every waveguide is $20\ \mu\text{m}$ long, $330\ \text{nm}$ wide and $300\ \text{nm}$ high. **b** Schematic of the shown structure

Two phase-coupled SPP modes are excited at the lower right and left edges of the input waveguides, so that SPPs are propagating diagonally upwards. In the intersection region, SPPs are coupled into the upward directed waveguide, depending on the phase shift between them. This waveguide is named the output waveguide in the following. Backscattering, i.e., SPP waveguide modes propagating downwards in the diagonal input waveguides and coupling into other directions (left, right, bottom), is suppressed.

Additionally, the coupling efficiency into the output waveguide can be tuned from zero to a maximum value with high precision, depending on the relative phase delay between the incoming SPPs in the input waveguides. Using this effect, SPP autocorrelation and SPP switching as a basic process for logic operational elements and circuitry are demonstrated. Furthermore, we demonstrate that the output efficiency of such waveguide structures can be increased and its functionality can be extended by varying the intersection angle of the input waveguides. Finally, an example for coherent SPP switching into different waveguide directions is presented.

Interferometric devices for multi-mode switching operation have been reported widely in previous literature [39, 40]. These multi-mode interferometers exceed several tens of micrometers in length. In contrast, the investigated structures in this paper exploit the fundamental SPP waveguide mode, enabling structural sizes in ranges of the wavelength.

2 Experimental details

2.1 Preparation of structures

The dielectrically loaded waveguiding structures for SPPs which are shown and investigated in this paper have been fabricated from the organic-inorganic hybrid photosensitive low shrinkage polymer Ormosil [41]. The bulk Ormosil

material has high optical transparency and a refractive index of about $n = 1.52$ in the near-infrared spectral range. The photopolymer Ormosil has been spin-coated to a layer thickness of 300 nm on top of a 50 nm gold film which has been deposited on a standard microscopic cover glass by thermal evaporation.

Afterward, the Ormosil has been lithographically structured using a two-step projection lithography approach. In the first processing step, the required structures have been designed on a computer and printed as a simple black-and-white image onto standard A4 copy transparencies. Subsequently, this transparency has been optically demagnified by a factor of 10:1, using illumination at a wavelength of 410 nm from a high-power LED source (ENFIS). The structures have been imaged onto a chromium-covered glass substrate with 25 mm diameter and 1 mm thickness which has been coated with positive-tone photoresist S1805 (Dow Chemical). After illumination, the photoresist has been developed, where the illuminated areas have been dissolved in an aqueous basic solution. The chromium layer with a thickness of 100 nm has subsequently been etched, producing an intermediate mask. This mask has further been optically demagnified by a factor of 100:1 in an inversely operated standard microscopy setup using a 100 \times microscope objective with a numerical aperture (NA) of 1.4 (Zeiss) for the generation of waveguide structures in Ormosil. The latter method of microscope projection photolithography (MPP) has originally been described in Refs. [42, 43]. Here, using the same method together with lithographic pre-processing of the mask, we demonstrate simple, low-cost, and high-resolution fabrication along with functionality of the generated structures.

Experimentally, the microscope demagnification has been realized by placing the mask in the image plane of the microscope objective with backside illumination by 365 nm radiation from a high-power UV LED (Roithner). The demagnified image has been projected onto the Ormosil layer, and UV radiation locally initiated a polymerization process. After development of the sample in isopropanol, the cross-linked material remained on the gold-covered glass substrate, whereas the unilluminated material has been washed out. This method allows fast and flexible production of arbitrary 2D structures with resolutions down to 230 nm [44].

The resulting structures, used in further investigations, consist of four 20- μm -long waveguides, rotationally separated by 45 $^\circ$ and intersecting at one single point. The width of the waveguides has been chosen for single-mode operation at optical excitation wavelengths of 800 nm in air. The effective mode index for the fundamental SPP in a 330-nm-wide and 300-nm-high waveguide has been determined by the finite element method (RSoft, FEMSim) to be 1.21. This value perfectly matches later experimental results described

in Sect. 3.3. The SPP wavelength in the waveguides has therefore been calculated as $800\text{ nm}/1.21 = 661.16\text{ nm}$, which is about twice the waveguide width, guaranteeing single-mode operation.

The geometrical characteristics, i.e., width and height, of the waveguides have been investigated and confirmed by scanning electron microscopy (SEM) (Quanta 400 FEG, FEI). The intersecting waveguides, shown in Fig. 1a, provide further information on the resolution of the fabrication process. Similar to a Siemens star, the minimal achievable resolution can be obtained by measuring the radius of curvature of the polymer at the intersection point between two neighboring waveguides. This minimal radius of curvature of 235 nm has been determined from the SEM images, in good agreement with the results described in [44]. The diameter of the waveguide junction in Fig. 1a has been measured to 1.2 μm .

2.2 Investigation techniques

Optical characterization of the waveguides, SPP transmission measurements, and investigation of coherent SPP interference interactions have been performed using leakage radiation microscopy (LRM) [22, 35, 45–49]. The 100 \times oil immersion microscopy objective (Zeiss) with a NA of 1.4, which has been used in the experimental setup for LRM, enables effective refractive indices up to 1.4 to be measured. The method has been upgraded by a 4f-lens system in the optical beam path to permit simultaneous observation of the image plane and the back focal plane. The latter is also commonly regarded as the Fourier transformation of the image with respect to emission angles of the SPP leakage radiation.

As laser source for SPP excitation, a mode locked titanium-sapphire oscillator (Kapteyn Murnane Labs) at 800 nm center wavelength and 40 nm spectral width, resulting in a Fourier-limited pulse duration of 27 fs, has been used. The beam has been focussed onto the waveguide sample by an aspheric lens with 4 mm focal length and 0.55 NA, giving a diffraction limited focal spot diameter of 750 nm. SPPs and SPP waveguide modes have locally been excited by focussing laser beam onto the waveguide edges. The effective unconfined SPP index and the confined SPP mode indices have directly been determined from the back focal plane images [47] to be 1.04 and 1.21, respectively. The experimental measurements are in detail described in Sect. 3.3.

In order to excite two phase-coupled SPP modes inside different waveguides, two replicas of the oscillator pulses have been generated using a Michelson interferometer. Both arms of the interferometer have been equipped with waveplates and tiltable mirror mounts, enabling independent adaptable polarization states and spatially adjustment

of both laser spots. The mirror mounts in turn have been attached to translation axes, for movement of the retro-reflecting mirrors parallel to the laser beam. This allows individual tuning of the optical path length of both arms and thus a time delay of the respective pulses. We will refer this optical path length difference as phase delay for changes below the wavelength, which induces a time delay below one optical cycle, whereas we will refer to it as time delay for changes bigger than the wavelength, respective one optical cycle. Via iterative tuning of the optical path length during observing the response on the sample, a tuning resolution around a phase shift of $\text{Pi}/3$ could be achieved.

3 Results and discussion

3.1 Excitation of SPPs with two laser spots and induced switching effects

For basic investigations, two SPP modes have been excited at the left and right lower edges of the input waveguides, pointing diagonally upwards in the star-like junction structure, as it is indicated in Fig. 2a. The polarizations of the incoming laser pulses have been set such that the electric field directions point along the axes of the two diagonal waveguides.

First, we consider SPP excitation in only one input waveguide. At the waveguide junction, the SPPs from a single-diagonal waveguide couple only weakly into the horizontal waveguides, pointing to the left and to the right and in the vertical upward waveguide. This is demonstrated in Fig. 2b, where only SPPs in the right upward directed input waveguide have been excited. The preferred propagation of SPPs inside the waveguide is straightforward along the diagonal direction of the input waveguide (see Fig. 2b). This straightforward propagation of the SPP mode is also the reason that no SPP back-reflection occurs, which will be further discussed in Sect. 3.3 of this paper. Coupling of SPPs into the horizontal right and upward waveguides has been found to be only weak.

The further obtainable intensity modulation in the vicinity of the junction point may be due to the ability of the SPP waveguide mode to couple into scattered light in the waveguide crossing. This scattered light can interfere with the leakage radiation causing the intensity modulations. The underlying effect was described by Hohenau et al. in detail [50]. In addition, the abrupt change in refractive index at the waveguide ends causes reflections, which is visible as intensity modulations at the waveguide ends. However, this reflected mode decays fast and is not visible at the input ports.

When both diagonal input waveguides have been excited, strong interference at the waveguide intersection

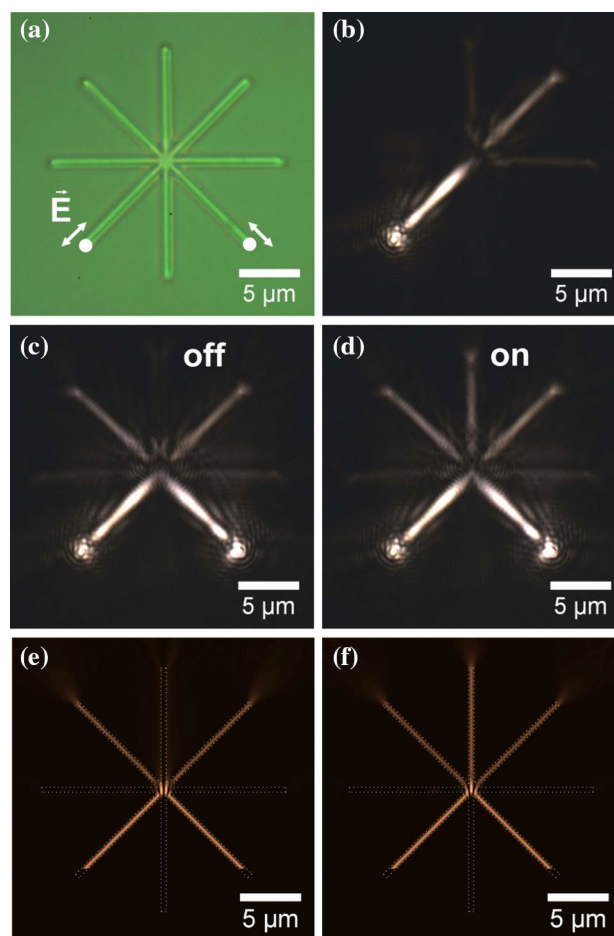


Fig. 2 a Brightfield LRM image of the investigated waveguide structure on a *thin gold layer*-coated standard microscopic cover glass. b–d Darkfield LRM images where in (b) SPP is excited at only one point and in (c, d) SPPs are excited at two points with 1 Pi phase shift (c) or 0 Pi phase shift (d) between the exciting laser spots. e, f numerical FDTD simulated images, respectively

point has been observed when two pulses perfectly overlap in time (no phase delay). The intensity of the two corresponding excitation laser beams has been adjusted equally.

Since the excitation is coherent, the relative phase of both SPPs in the input waveguides can be varied using the Michelson interferometer, resulting in variable interference patterns at the intersection. This, in turn, affects the intensity of the SPP mode excited in the output waveguide. LRM images of this effect are presented in Fig. 2c, d, respectively.

When both SPPs are in phase (see Fig. 2d), interference in the intersection area leads to periodic field oscillations longitudinal to the straight upward and downward waveguides. Since the SPPs wave vectors in both input waveguides point diagonally upwards, energy coupling is better phase-matched into the upward (output) waveguide. No wave vector component is pointing into the downward

directions, therefore no SPP signal in the downward waveguide, and no back-reflections into the input waveguides occur as it is shown in Fig. 2d.

Varying now the relative phase between SPPs such that the phase difference becomes equal to π , the interference of the two modes leads to SPP field oscillations in the junction point, which are perpendicular to the output waveguide. That means that no SPPs are excited into the upward and downward waveguides (see Fig. 2c).

This effect could be employed for SPP switching purposes, whereas the response rate is dependent on the time scales of phase changes of the excitation laser pulses. Recent publications report optical pulse shaping, with a varying phase over ultrafast pulse durations [51], which is able to be deployed in the THz regime [52]. Rudé et al. recently reported a structural phase-changing technique for phase changes below 500 fs, persisting for about 3 ps in [53]. Nonlinear direct modulation of SPP phases at femto-second time scales is reported in [54]. Thus, the described switching effect can take place in the ultrafast time regime.

However, compared to other SPP interference approaches discussed in [36], the advantage of the here presented scheme is the completely avoided backscattering. Furthermore, the contrast between the signals in the output waveguide in the *on* and *off* states can be very high.

The intensity contrast between the *on* and *off* states has been found to be 13 dB using experimental LRM measurements. Numerical simulations based on finite-difference time-domain (FDTD) computation [35, 55–57] have revealed a contrast value of 23 dB for ideal waveguides geometry. The difference between experimental and numerical results is due to the 8-bit limited dynamics of the CMOS camera in the LRM setup, resulting in a maximum dynamic range of 24 dB. Therefore, only little amounts of scattered light can drastically reduce the measurable contrast.

Further, for the *on* state, the signal intensity at the output waveguide exit is only 1.5 dB lower than the signal intensity at the exit ends of the input waveguides, both, in experiments and simulations.

The overall losses of the SPP waveguide mode resemble a propagation ($1/e$) length of 7 μm . This is in very good agreement to values in literature for this type of waveguides, e.g., 6.5 μm presented in [23]. It is to say that the investigated plasmonic system is not optimized for lowest possible losses but for best possible interpretability of the images, made with the introduced LRM system. Changing the used wavelength [24] or using thicker gold [58] could enhance the propagation length drastically.

A sweep of the time delay between two fs laser pulses used for excitation of SPPs yields different intensities in the output waveguide. Every intensity maximum and minimum of a sweep over the whole pulse duration returns an

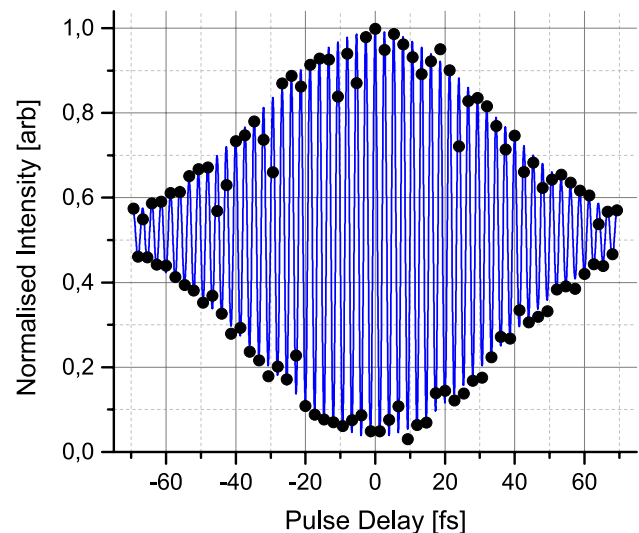


Fig. 3 Autocorrelation function for the experimental conditions as in Fig. 2: Two SPPs have been excited with two fs laser pulses (Fourier-limited pulse duration 27 fs) at the lower ends of the diagonal waveguides. During the experiment, one laser pulse has been fixed, whereas the optical path of the second laser pulse has been lengthened manually in steps of 400 nm, which corresponds to the temporal delay of 1.33 fs per step. The experimental obtained maxima and minima of the SPP intensity in the output waveguide are shown as *black dots*. As a *blue curve*, theoretical autocorrelation function of the first order for gaussian pulses with an intensity FWHM of 39 fs has been calculated

intensity autocorrelation function of first order for SPP. The result presenting the obtained autocorrelation curve, normalized to unity, is plotted in Fig. 3 as black circles.

A theoretical autocorrelation curve of the first order has been calculated for an assumed temporal gaussian SPP pulses with an intensity full width at half maximum (FWHM) of 39 fs. The theoretical curve has been added to the experimental results as blue curve, showing a very good agreement.

It should, however, be noted that we do not relate the discrepancy in laser oscillator pulse duration (27 fs) and the SPP pulse duration (39 fs) revealed from the theoretical fit to pulse broadening effects, since the first-order autocorrelation function does not provide pulse duration information for chirped pulses. Therefore, the actual SPP pulse characteristics on the waveguide sample surface are not known in this experiment. We consider that the pulse duration of the excited and propagating SPPs remains ultrafast in the sub-75 fs region, since after setting the pulse delay higher than 75 fs no interference effects can be observed.

The autocorrelation curve in (Fig. 3) proves that all measured effects are of linear nature and that nonlinear processes are not involved in the switching of the output waveguides state.

For the region of nearly perfect temporal overlap, a more detailed investigation of the phase shift dependence of the

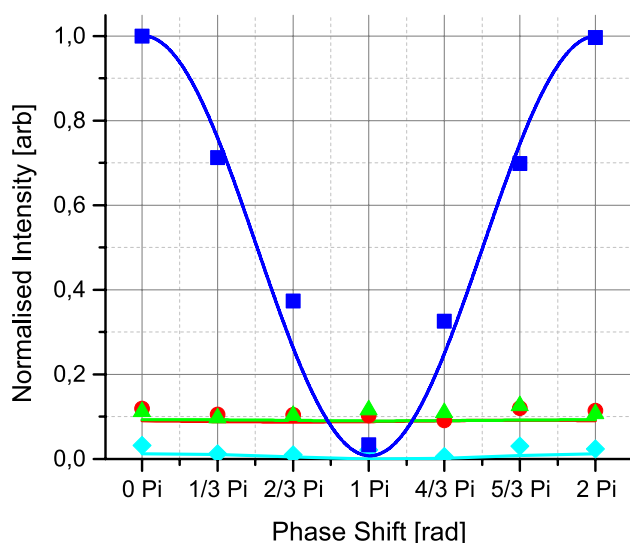


Fig. 4 Experimentally (points) and numerically simulated FDTD (lines) results of a phase sweep in steps of $\text{Pi}/3$ for the same experimental conditions as in Fig. 2c, d. The blue squares represent the intensity of the output waveguide. The red circles and green triangles show the intensity in the left and right waveguides, and the cyan diamonds show the intensity in the downward directed waveguide. The blue, green, red and cyan lines are simulated results, respectively

SPP intensities in horizontal and vertical waveguides has been performed. The phase of one excitation laser pulse has been tuned in steps of $\text{Pi}/3$, whereas the phase of the other laser pulse has been fixed. The experimental results of the phase variation show a clear cosine-dependence of the intensity in the output waveguide, as it is given by the blue squares in Fig. 4. The intensities of the left and right propagating SPPs are depicted by red circles and green rectangles in the same figure. One can see that the intensity in the left and right waveguides is only weakly dependent on the relative phase of the coherent SPPs in the input waveguides.

The intensity of the SPP in the downward directed waveguide is shown with the cyan diamonds in Fig. 4, and it provides the lowest measured signal. In these measurements, the background signal has been subtracted in all results. The experiment has been compared with a numerical FDTD simulation. The results are shown by the solid lines in Fig. 4 and are in good agreement with the experimentally obtained data.

Slight differences between simulated and measured intensities may be due to the finite resolution of the fabrication process, which produces imperfect intersections between two waveguides. The intersections in the numerical simulations have been assumed as infinitely sharp, as it is given by the projection mask layout.

The observed interference effect within the investigated structure can be considered as an ultrafast switch

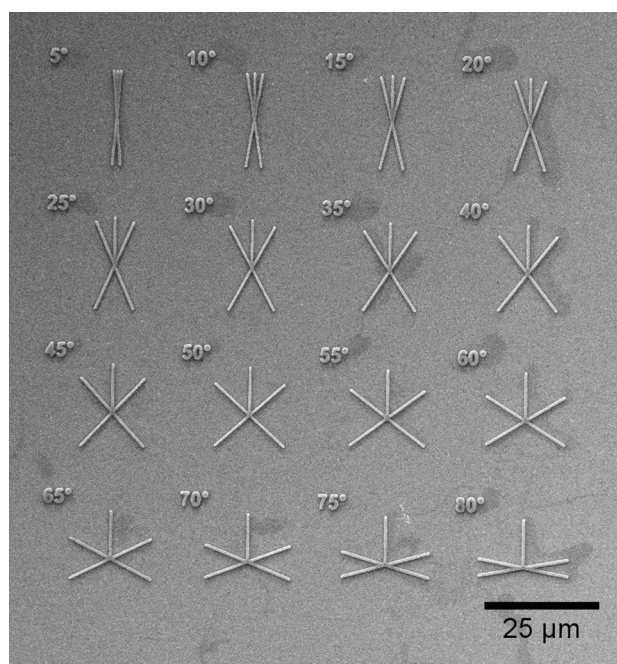


Fig. 5 Scanning electron microscope image of the structures used for investigations of the angle dependence between the waveguides. The diagonal waveguides are $20\ \mu\text{m}$ and the vertical waveguides $10\ \mu\text{m}$ long. All waveguide structures are $330\ \text{nm}$ wide and $300\ \text{nm}$ high. The lithographically written numbers refer to the angle between the diagonal and vertical waveguides, respectively

for SPP propagation. Furthermore, the operation of the waveguide junction already resembles a logic AND gate. The switching effects between two input waveguides can further be extended for the realization of logic OR and XOR gates.

3.2 Different angles between input and output waveguides

As a next step, the dependence of the output signal intensity on the angle between input and output waveguides has been investigated. New structures with two $20\text{-}\mu\text{m}$ -long diagonal input waveguides and one $10\text{-}\mu\text{m}$ -long vertical output waveguide, shown in Fig. 5, have been produced by MPP. The width and height of the waveguide structures have been again set to 330 and $300\ \text{nm}$, respectively. The individual structures have been designed with different angles between the input and output waveguides to investigate the angular dependence of the intensity of the SPP signal intensity in the vertical output waveguide.

Two coherent laser pulses have been focused on the lower ends of the input waveguides, while a phase difference of $0\ \text{Pi}$ has been maintained between them. The SPP intensity in the output waveguide has been measured. The results have again been compared with numerical FDTD

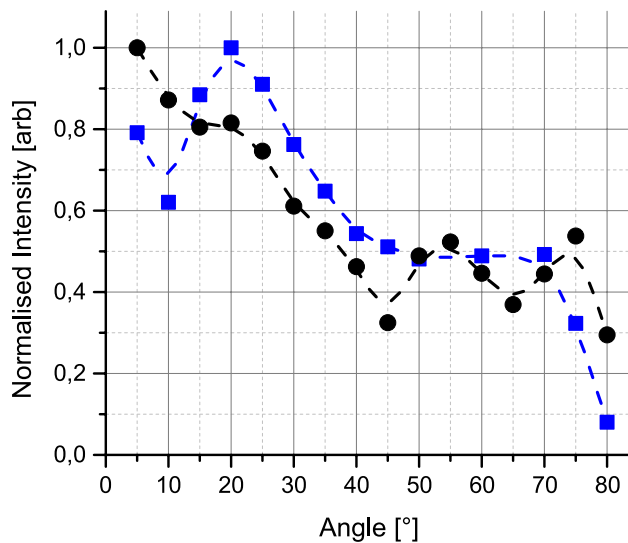


Fig. 6 Comparison of numerically simulated (blue squares) and experimental (black circles) results of the SPP intensities in the vertical waveguides of the structures shown in Fig. 5. The squares and circles are the measured results, whereas the dashed lines are approximations for eye guidance only

simulations. Both results are plotted in Fig. 6, indicating good agreement between the experimental (black circles) and numerical (blue squares) data. Both results have been normalized to their maximum values. The obtained results clearly show that there is a strong dependence of the SPP intensity in the output waveguide on the angle between the input and output waveguides. The output signal is considerably higher in case of smaller angles. In the simulations, a maximum of the output signal for 20° has been found.

3.3 Proof of the avoided backscattering in the Fourier plane

LRM images of the 20° and 55° structures and the corresponding Fourier transformations can be seen in Fig. 7a, c (image plane) and Fig. 7b, d (Fourier plane). It is clearly visible in the image plane (Fig. 7a, c), that for 20° angle the intensity of the SPP in the vertical output waveguide is much higher.

In the Fourier plane images shown in Fig. 7c, d, one can see bright circles with the effective refractive index of $n_{\text{eff}} = 1.04$. This circles reveal the angular distribution of the leakage radiation of free propagating SPP modes on the thin gold layer. Furthermore, Fig. 7b, d shows in the upper region bright fringes with $n_{\text{eff}} = 1.21$, revealing the angular dependence of the leakage radiation of the confined propagating SPP modes in the waveguide structure. It should be noted that there is no signature of confined SPP modes in

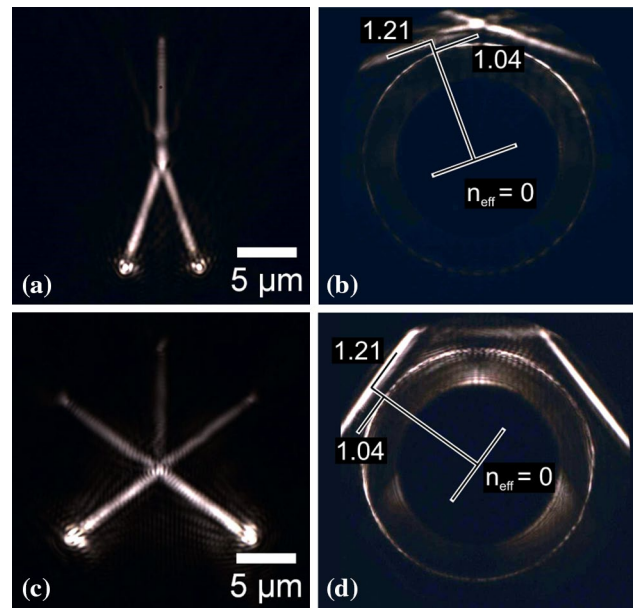


Fig. 7 a, c Darkfield LRM images of the 20° and 55° angle structures from Fig. 5 with no phase difference at the inputs. b, d Corresponding images in the Fourier plane. The effective refractive index n_{eff} of the SPP mode signatures are related to the emission angle of the leakage radiation of the confined ($n_{\text{eff}} = 1.21$) and unconfined ($n_{\text{eff}} = 1.04$) SPP modes

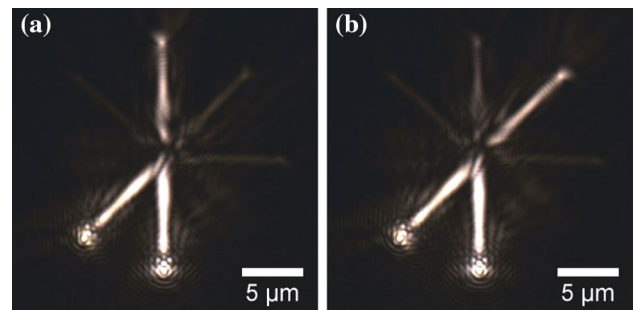


Fig. 8 Darkfield LRM images of SPPs excited at two different waveguide endpoints. Due to a phase shift between two SPPs, the SPP output can be switched between different waveguides in the upward direction (a) and right diagonal direction (b)

the lower region of the Fourier planes, which would have their origin in confined backward propagating SPP modes in the lower three waveguides. Thus, no signal backscattering or back-reflection in any downward direction occurs, which is one of the requirements for a successful operation and cascability of logical optical elements.

By varying the angle between the waveguides, the transferred energy to the output waveguide has been experimentally optimized. This is an important step to drive at least two new inputs with one output (fan-out).

3.4 Excitation of different waveguides

By changing the in-coupling geometry of two coherent SPPs in the multiple waveguide junction shown in Fig. 2a, different propagation and switching effects can be observed. As an example, SPPs in one diagonal and the vertical waveguides have been excited, as it is shown in Fig. 8. In this case, the output signal can be switched nearly completely into the diagonal or vertical output waveguides.

4 Conclusion

In conclusion, SPP propagation properties in a multiple crossing waveguide junction have been investigated using leakage radiation microscopy. Potential applications of such waveguide junction as an ultrafast plasmonic switch and a basic element for the realization of plasmonic logic gate structures have been demonstrated. It has been found that SPP propagation into certain output waveguides can be coherently controlled by adjusting the relative phase delay between two input SPPs. Furthermore, it has clearly been shown that backscattering and back-reflections at the waveguide junction are completely avoided. Additionally, it has been shown that the SPP intensity in the output waveguide can be significantly increased by optimizing the intersection angle between the input and output waveguides. This provides possibilities for cascading two or more basic elements to obtain complex optical logic circuitry. Experimental results have been supported by numerical FDTD simulations yielding good agreement with our observations.

Acknowledgments The authors acknowledge financial support of this work from the Deutsche Forschungsgemeinschaft (DFG: SPP 1391 “Ultrafast Nanooptics”, SFB/TRR 123 “Planar Optronics Systems” and EV 220/2-1) and support of the Laboratory of Nano and Quantum Engineering (LNQE). The authors further acknowledge support from Hannover School of Nanotechnology (HSN).

References

- C. Lu, X. Hu, H. Yang, Q. Gong, *Sci. Rep.* **3** (2013)
- H. Wei, Z. Wang, X. Tian, M. Kil, H. Xu, *Nat. Commun.* **2**, 387 (2011)
- S.K. Kwong, G.A. Rakuljic, A. Yariv, *Appl. Phys. Lett.* **48**, 201 (1986)
- Y. Fainman, C.C. Guest, S.H. Lee, *Appl. Opt.* **25**, 1598 (1986)
- M. Ogusu, S. Tanaka, K. Kuroda, *Jpn. J. Appl. Phys.* **29**, L1265 (1990)
- V.R. Almeida, C.A. Barrios, R.R. Panepucci, M. Lipson, *Nature* **431**, 1081 (2004)
- Y. Zhang, Y. Zhang, B. Li, *Opt. Express* **15**, 9287 (2007)
- Q.F. Xu, M. Lipson, *Opt. Express* **15**, 924 (2007)
- J. Zhang, K.F. MacDonald, N.I. Zheludev, *Light Sci. Appl.* **1**, e18 (2012)
- X. Fang, M.L. Tseng, J.Y. Ou, K.F. MacDonald, D.P. Tsai, N.I. Zheludev, *Appl. Phys. Lett.* **104**, 141102 (2014)
- X. Fang, K.F. MacDonald, N.I. Zheludev, *Light Sci. Appl.* **4**, e292 (2015)
- H.J. Caulfield, J. Westphal, *Inf. Sci.* **162**, 21 (2004)
- L. Qian, H.J. Caulfield, *Inf. Sci.* **176**, 3379 (2006)
- W.L. Barnes, A. Dereux, T.W. Ebbesen, *Nature* **424**, 824 (2003)
- T.W. Ebbesen, C. Genet, S.I. Bozhevolnyi, *Phys. Today* **61**, 44 (2008)
- H. Wei, Z. Li, X. Tian, Z. Wang, F. Cong, N. Liu, S. Zhang, P. Nordlander, N.J. Halas, H. Xu, *Nano Lett.* **11**, 471 (2011)
- Y. Fang, M. Sun, *Light Sci. Appl.* **4**, e294 (2015)
- S.I. Bozhevolnyi, V.S. Volkov, E. Devaux, J.-Y. Laluet, T.W. Ebbesen, *Nature* **551**, 508 (2006)
- S.I. Bozhevolnyi, J. Jung, *Opt. Express* **16**, 2676 (2008)
- E. Verhagen, J.A. Dionne, L. Kuipers, H.A. Atwater, A. Polman, *Nano Lett.* **8**, 2925 (2008)
- E. Verhagen, M. Spasenovic, A. Polman, L. Kuipers, *Phys. Rev. Lett.* **102**, 203904 (2009)
- C. Reinhardt, R. Kiyon, S. Passinger, A.L. Stepanov, A. Ostendorf, B.N. Chichkov, *Appl. Phys. A* **89**, 321 (2007)
- J. Grandidier, S. Massenet, G.C. Des Francs, A. Bouhelier, J.C. Weeber, L. Markey, Dereux, J. Renger, M.U. Gonzalez, R. Quindant, *Phys. Rev. B Condens. Matter Mater. Phys.* **78**, 1 (2008)
- A. Seidel, C. Reinhardt, T. Holmgaard, W. Cheng, T. Rosenzweig, K. Leosson, S.I. Bozhevolnyi, B.N. Chichkov, *IEEE Photonics J.* **2**, 652 (2010)
- P. Berini, R. Charbonneau, N. Lahoud, *Nano Lett.* **7**, 1376 (2007)
- P. Berini, *Adv. Opt. Photonics* **1**, 484 (2009)
- V.S. Volkov, Z. Han, M.G. Nielsen, K. Leosson, H. Keshmiri, J. Gosciniak, O. Albrechtsen, S.I. Bozhevolnyi, *Opt. Lett.* **36**, 4278 (2011)
- S.A. Maier, P.G. Kik, H. Atwater, S. Meltzer, E. Harel, B.E. Koel, A.G. Requicha, *Nat. Mater.* **2**, 229 (2003)
- A.B. Evlyukhin, S.I. Bozhevolnyi, *Laser Phys. Lett.* **3**, 396 (2006)
- A.B. Evlyukhin, C. Reinhardt, E. Evlyukhina, B.N. Chichkov, *Opt. Lett.* **34**, 2237 (2009)
- D. Van Orden, Y. Fainman, V. Lomakin, *Opt. Lett.* **34**, 422 (2009)
- S.I. Bozhevolnyi, J. Erland, K. Leosson, P.M.W. Skovgaard, J.M. Hvam, *Phys. Rev. Lett.* **86**, 3008 (2001)
- T. Søndergaard, S.I. Bozhevolnyi, *Phys. Rev. B* **67**, 165405 (2003)
- A. Markov, C. Reinhardt, B. Ung, A.B. Evlyukhin, W. Cheng, B.N. Chichkov, M. Skorobogatiy, *Opt. Lett.* **36**, 2468 (2011)
- C. Reinhardt, A.B. Evlyukhin, W. Cheng, T. Birr, A. Markov, B. Ung, M. Skorobogatiy, B.N. Chichkov, *J. Opt. Soc. Am. B* **30**, 2898 (2013)
- Y. Fu, X. Hu, C. Lu, S. Yue, H. Yang, Q. Gong, *Nano Lett.* **12**, 5784 (2012)
- C. Lu, X. Hu, S. Yue, Y. Fu, H. Yang, Q. Gong, *Plasmonics* **8**, 749 (2013)
- D.B. Miller, *Nat. Photonics* **4**, 3 (2010)
- L.B. Soldano, E.C.M. Pennings, *J. Lightwave Technol.* **13**, 615 (1995)
- A. Ortega-Moñux, C. Alonso-Ramos, A. Maese-Novo, R. Halir, L. Zavargo-Peche, D. Pérez-Galacho, I. Molina-Fernández, J.G. Wangüemert-Pérez, P. Cheben, J.H. Schmid, J. Lapointe, D. Xu, S. Janz, *Laser Photonics Rev.* **7**, 12 (2013)
- A. Ovsianikov, J. Viertl, B. Chichkov, M. Oubaha, B. MacCraith, I. Sakellari, C. Fotakis, *ACS Nano* **2**, 2257 (2008)
- H. Kawata, J.M. Carter, A. Yen, H.I. Smith, *Microelectron. Eng.* **9**, 31 (1989)
- J.C. Love, D.B. Wolfe, H.O. Jacobs, G.M. Whitesides, *Langmuir* **17**, 6005 (2001)

44. C. Reinhardt, V.F. Paz, L. Zheng, K. Kurselis, T. Birr, U. Zywi-etz, B. Chichkov, K. Frenner, W. Osten, in *Optically Induced Nanostructures: Biomedical and Technical Applications*, ed. by K. König, A. Ostendorf (Walter de Gruyter GmbH & Co KG, 2015)
45. C. Reinhardt, R. Kiyam, A. Seidel, S. Passinger, A.L. Stepanov, A.B. Evlyukhin, B.N. Chichkov, in *Proceedings of SPIE 6642, Plasmonics: Nanoimaging*, 664205 (2007)
46. A. Drezet, A. Hohenau, D. Koller, A. Stepanov, H. Ditlbacher, B. Steinberger, F.R. Aussenegg, A. Leitner, J.R. Krenn, *Mater. Sci. Eng. B Solid State Mater. Adv. Technol.* **149**, 220 (2008)
47. C. Reinhardt, A. Seidel, A.B. Evlyukhin, W. Cheng, B.N. Chichkov, *J. Opt. Soc. Am. B* **26**, B55 (2009)
48. C. Reinhardt, A. Seidel, A. Evlyukhin, W. Cheng, R. Kiyam, B. Chichkov, *Appl. Phys. A Mater. Sci. Process.* **100**, 347 (2010)
49. N. Sardana, T. Birr, S. Schlenker, C. Reinhardt, J. Schilling, *New J. Phys.* **16**(6), 63053 (2014)
50. A. Hohenau, J.R. Krenn, Drezet, O. Mollet, S. Huant, C. Genet, B. Stein, T.W. Ebbesen, *Opt. Express* **19**, 25749, (2011)
51. C. Schwarz, O. Hütter, T. Brixner, *J. Opt. Soc. Am. B* **32**, 933–945 (2015)
52. A.M. Weiner, *Opt. Commun.* **284**, 3669–3692 (2011)
53. M. Rud, V. Mkhitaryan, A.E. Cetin, T.A. Miller, A. Carrilero, S. Wall, F.J.G. de Abajo, H. Altug, V. Pruneri, arXiv:1506.03739, 119 (2015)
54. K.F. MacDonald, Z.L. Samson, M.I. Stockman, N.I. Zheludev, *Nat. Photonics* **3**, 55–58 (2008)
55. A. Taflove, S.C. Hagness, *Computational Electrodynamics: The Finite-Difference Time-Domain Method*, 3rd edn. (Artech House, Boston, 2005)
56. C. Lemke, C. Schneider, T. Leissner, D. Bayer, J.W. Radke, A. Fischer, P. Melchior, A.B. Evlyukhin, B.N. Chichkov, C. Reinhardt, M. Bauer, M. Aeschlimann, *Nano Lett.* **13**, 1053 (2013)
57. C. Lemke, T. Leissner, A.B. Evlyukhin, J.W. Radke, A. Klick, J. Fiutowski, J. Kjelstrup-Hansen, H.-G. Rubahn, B.N. Chichkov, C. Reinhardt, M. Bauer, *Nano Lett.* **14**, 5 (2014)
58. A. Kolomenski, A. Kolomenskii, J. Noel, S. Peng, H. Schuessler, *Appl. Opt.* **48**, 5683 (2009)